New Insight on Initiation of Cavitation in Semicrystalline Polymers: In−Situ SAXS Measurements

ARTICLE *in* MACROMOLECULES · JULY 2010

Impact Factor: 5.8 · DOI: 10.1021/ma101042d

5 AUTHORS, INCLUDING:

Olivier Lame
Institut National des Sciences Appliquées de…
50 PUBLICATIONS **514** CITATIONS
SEE PROFILE

Jean-Marc Chenal
Institut National des Sciences Appliquées de…
50 PUBLICATIONS **365** CITATIONS
SEE PROFILE

DOI: 10.1021/ma101042d

Macromolecules
ARTICLE

New Insight on Initiation of Cavitation in Semicrystalline Polymers: In-Situ SAXS Measurements

S. Humbert,[†] O. Lame,*[,†] J. M. Chenal,[†] C. Rochas,[‡] and G. Vigier[†]

[†]*MATEIS−CNRS UMR5510, Bâtiment Blaise Pascal, INSA-Lyon, F-69621, Villeurbanne, France, and* [‡]*CERMAV-CNRS BP 53-38041, Grenoble cedex 9, France*

Received May 17, 2010; Revised Manuscript Received July 6, 2010

ABSTRACT: The phenomenon of cavitation generally appears close to yielding in the high-density polyethylene. It can affect the yield stress and the properties at large strains. The influence of the microstructural and molecular parameters on cavitation is not well established; it is not even clear whether the cavitation is a cause or a consequence of plasticity. In this work, we focus on the initiation of cavitation and on the nucleation rate. Various polyethylenes with a wide range of microstructural and molecular parameters have been obtained. The cavitation is followed up by SAXS in-situ tensile tests. It is found that, depending on the polyethylene, cavitation can be avoided or, on the contrary, appears before or after yielding. The stresses necessary to initiate cavitation and crystallite shearing have been relied respectively on stress transmitters (tie molecules, interphase, etc.) and crystallite thickness. Then the comparison between the materials has allowed predicting the various polyethylene behaviors. All of the latter have been explained by a simple model based on very few microstructural parameters. Surprisingly, our results have shown that all the scenarios of plasticity and cavitation are possible. One is the cause or the consequence of the other in accordance with the molecular topology and the microstructure.

Introduction

Deformation of the semicrystalline polymers has been the topic of many studies for the past 40 years, especially on polyethylene. Among various topics, the yielding behavior and cavitations turn out to be major issues.[1−11] It is reported in the literature that cavitations can be concomitant with yielding, as cavity formation is necessarily a damage. Indeed, the comparison of a tensile test with a compression[3] which avoids cavitation has allowed concluding that cavitation can affect the macroscopic yield stress.

Therefore, the question of interaction between cavitation and yielding is raised. It is crucial to take into account cavitations to predict the mechanical behavior of polyethylene and probably of all the semicrystalline polymers.

Cavitations can be studied by the SAXS technique.[1−4] General ideas are well established such as the evolution of the shape and the orientation of the cavities during the tensile test. The onset of cavitation generally occurs around the macroscopic yield point, and cavities are supposed to be formed in the amorphous phase, in the neighborhood of the crystalline phase or even at the interface crystal/amorphous phase. At the very beginning, the cavities are ellipsoidal, oriented perpendicular to the tensile direction. Then, during necking the cavity volume increases significantly. Finally, during the plateau, the cavities are elongated and oriented along the tensile direction. However, several points are still controversial, such as the initiation of cavitation and its role in the plastic deformation. Butler[1] has observed that the cavitation occurs from the yield point, which suggests that cavity formation is a consequence of the crystallite shearing. But this analysis is contradicted by the works of Pawlak and Galeski.[2,3] Because of the visible influence of cavitation on the yield stress value, they conclude that the cavities appear just before the yield stress and then modify the stress value. The cavities would be in this case an initiator of the plasticity. In addition, it has to be mentioned that cavitation is not present for all the polyethylenes. In particular, the quenched polyethylenes or those with thinnest crystalline lamellae do not exhibit any cavitation.[2,3,12]

As explained by Pawlak and Galeski, the crystallite thickness influences the yield stress. Increasing the crystalline thickness leads to a higher stress which promotes the initiation of cavitations. The influence of molecular parameters has also been evoked. The cavity volume is found to be higher when the molecular weight is low.[1] Low molecular weights generate fewer entanglements during crystallization, which favors a larger amount of cavities. Moreover, the influence of the mobility of the amorphous phase is highlighted by Castagnet.[13] It is also likely that the entanglements and the tie molecules could influence the cavity formation as they modify the mobility in the amorphous phase.

It appears that it remains unclear whether the cavitation is a cause or a consequence of plasticity all the more they are certainly interacting.

The aim of this work is to bring some new clues to answer the latter questions, especially the precise implication of the molecular and microstructural parameters such as tie molecule and entanglement density and crystallite thickness.

Experiments are performed on several polyethylenes with controlled molecular parameters and subjected to different thermal treatments. Indeed, molecular topology differences coupled with various crystallization conditions allow obtaining a wide range of microstructural characteristics. The cavity formation will be mainly analyzed by SAXS in-situ tensile tests performed at the ESRF (European Synchrotron Radiation Facility). The initiation of cavitations will be also evaluated more qualitatively by whitening during the tensile test.

*Corresponding author: Tel (+33) 47-243-8357; Fax (+33) 47-243-8528; e-mail Olivier.lame@insa-lyon.fr.

 Published on Web 07/27/2010

Experimental Section

Materials. Four polyethylenes, obtained using the Phillips catalysis with a chromium oxide leading to a medium molar mass M_w (between 180 and 230 kDa), are studied. They differ from their molecular topology: their counit content differs from a sample to an other. The PE A and PE B have a higher hexene counit C6 content (respectively 1.8 and 0.8 mol %) (see Table 1) than the PE C and PE D (respectively 0.1 and 0.2 mol %). In each category, the polyethylenes differ from their crystallinity: the one of the PE A (49%) is lower than the one of the PE B (54%), and the same gap exists between the crystallinity of the PE C and PE D (respectively 65% and 69%).

Sample Preparation. 500 μm thick sheets are obtained from pellets molding between aluminum foils in a press at 170 °C. Then, the polymer sheets are quenched in water at a rate of ~30 °C/s. To modify the microstructure, isothermal crystallizations are performed with two different processes. Samples designated hereafter as "annealed" are heated from their quenched state to a temperature close to the crystallization temperature (see Table 2) and are held in these conditions in a thermostatic oil bath for about 15 h.

The samples called "isotherm" are remelted at 170 °C in an oven before being cooled in a thermostatic oil bath at a temperature close to the crystallization temperature (see Table 2) and held in these conditions for 15 h. Samples are tightly wrapped in order to avoid oil contamination from the thermostatic bath. Moreover, the infrared technique does not show a peak at 1720 cm^{-1} relating to the carbonyl groups and consequently probes that the oxidation is insignificant.

Characterization. *Tensile Measurements.* To observe the macroscopic deformation of the sample and the presence of the cavitation, tensile tests have been carried out. Dumbbell-shaped samples of 22 mm gauge length, about 5 mm width, and about 0.5 mm of thickness were cut from the sheets. A series of tests were performed with a MTS machine at 23 °C. They were carried out with a crosshead-speed constant, fixed in order to have an initial strain rate of 5×10^{-3} s^{-1} and to obtain nominal stress/strain curves. These tests allow measuring the natural draw ratio (λ_n) with the method of tangents.[6] They also allow photographing the sample every 15 s, which corresponds to a deformation of 7.5%.

SAXS. Small-angle X-ray scattering experiments were carried out on the CRG D2AM beamline of the European Synchrotron Radiation Facility (ESRF) (Grenoble, France).

The measurements were performed using a wavelength of 1.54 Å, allowing an observation range in q from 0.05 to 0.95 nm^{-1}. The SAXS patterns were recorded thanks to a 2D detector. The data corrections (dark current, flat field response, and tapper distortion) were carried out using the software available on the beamline. Silver behenate was used for the q-range calibration. Then, the data have been corrected from the fluctuation of the incident beam intensity and from the background.

The long period (L_p) was calculated from the maximum of the diffuse intensity corrected by the Lorentz factor ($Iq^2 = f(q)$) with the relation

$$L_p = \frac{2\pi}{q_{max}} \text{ (nm)} \quad (1)$$

with q_{max} corresponding to the peak maximum.

The thicknesses of the crystalline lamellae were deduced, with a precision of ±5%, from L_p and X_c (measured by differential scanning calorimetry) thanks to the following relations:

$$L_c = L_p \frac{\rho}{\rho_c} X_c \quad (2)$$

where ρ_c, the crystalline density, equals 1.003 g cm^{-3} and ρ is the density of the sample.[8]

Thanks to a homemade miniature stretching device, in-situ tensile tests were performed on dumbbell-shaped samples of gauge length 6.5 mm, width about 4 mm, and thickness of about 0.5 mm. The samples were stretched at an initial strain rate of 6.4×10^{-4} s^{-1}. The symmetric displacement of the two clamps allows probing the same zone during the tensile test. The pattern acquisition time was chosen in order to have a good compromise between the pattern quality and the smallest deformation as possible during the acquisition. Hence, the acquisition time was 5 s, which corresponded to a strain increase of about 0.3%.

Table 1. Initial Characteristics of the Different Polyethylenes[a]

material	C6 (mol %)	M_n (kDa)	M_w (kDa)	M_z (kDa)	I_p	X_c[b] (%)
PE A	1.8	14.3	231	2770	16.1	49
PE B	0.8	15.8	187	1770	11.9	54
PE C	0.1	15.4	216	2770	14	65
PE D	0.2	15	229	4100	15.3	69

[a] M_n, M_w, and M_z are respectively the number-average molar mass, the weight-average molar mass, and the z-average molar mass, and I_p is the polydispersity index (M_w/M_n). [b] After quenching.

Results and Discussion

Estimation of Stress Transmitter Density. Elements as tie molecules (TMs), entanglements, and possibly the partial percolation of the crystalline phase participate in the network which is likely essential to transmit the applied stress through the lamella stacks. Their mechanical contribution can hardly be dissociated by experimental methods, which is why we consider that they all belong to the same group of elements: the stress transmitters (ST). We have seen in a

Table 2. Characteristics of the Different Polyethylenes

type	material	Thermal treatment T(°C)	C6 %mol	Xc (%)	Lp (nm)	Lc (nm)	λn	Symbols
PE A	A quenched	/	1,8	49	17	8	**3,5**	■
	A annealed	114		52	23	11	**4**	■
	A isotherm	114		53	24	12	**4,75**	□
PE B	B quenched	/	0,8	54	19	9	**4,25**	◆
	B annealed	113		62	22	13	**4,75**	◆
	B isotherm	113		65	26	16	**5,5**	◇
PE C	C quenched	/	0,1	65	20	12	**4,5**	✱
	C annealed	124		73	30	21	**6**	✱
	C isotherm	124		75	36	26	**7,5**	✳
PE D	D quenched	/	0,2	69	22	14	**5**	▲
	D annealed	123		77	30	22	**5,75**	▲
	D isotherm	123		80	37	29	**7**	△

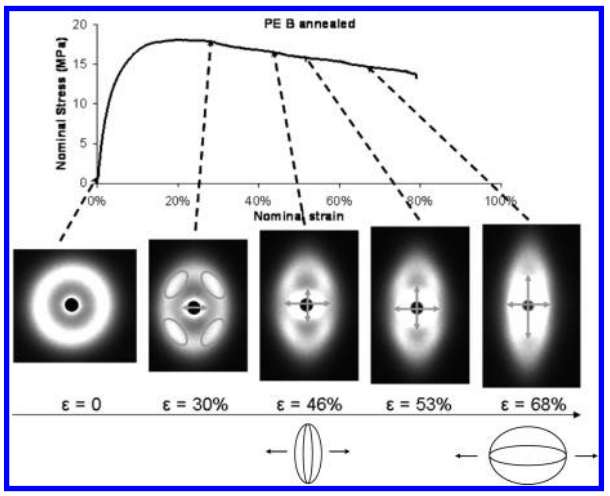

Figure 1. Evolution of the SAXS patterns along the tensile for the PE B annealed.

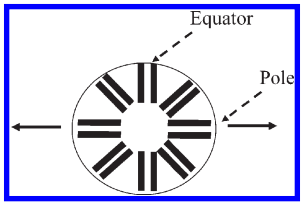

Figure 2. Scheme of a spherulite with its equatorial and polar regions.

previous work[6] that many methods could help evaluating the density of stress transmitters such as the strain hardening, the natural draw ratio, the neck width measured on the nominal stress/strain curve that is relevant of the plastic instability, and the statistical model of Brown.[14,15]

As all these methods give roughly the same evaluation, we have chosen to use in this study the natural draw ratio (λ_n) as it is considered to be correlated to the density of tie molecules and entanglements.[16,17] As λ_n decreases when the ST density increases, the ST density will be estimated and considered to be proportional $1/\lambda_n$.

Description of the Processus of Cavitation. *Observation of the Cavitation*. The phenomenon of cavitation is visible by the SAXS technique as the intensity scattered by the cavities is detectable at the low q values (see the arrows in Figure 1).

Except for the position of the onset of the cavitation, all the polyethylenes exhibit the same evolution of the shape and orientation of the cavities during the tensile test.

The behavior of the PE B annealed is presented in Figure 1 as an example. The direction of the tensile direction is horizontal. The acquisition was stopped when the scattered intensity was too strong. Indeed, cavities scatter much more than the lamella stacks, and thus, the intensity can overload the detector.

The equatorial and polar regions of the spherulite can be defined as follows: the longest direction of the lamellae in the equatorial regions is perpendicular to the tensile direction whereas it is parallel to the tensile direction in the polar regions (see Figure 2).

The horizontal and vertical zones (zones H and V) of the pattern are defined as shown in Figure 3: the horizontal zones of the detector are parallel to the tensile direction.

As described in the literature by Hubert et al.,[18] the two-dimensional SAXS initial pattern shows an isotropic scattering ring that is consistent with scattering from randomly oriented lamella stacks (see Figure 1). During stretching at small strains, the lamella stacks perpendicularly oriented to

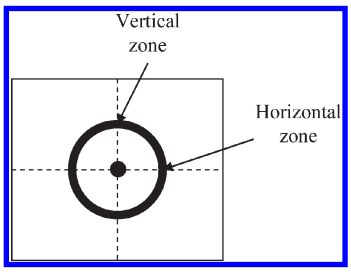

Figure 3. Scheme of a diffusion figure with its horizontal and vertical zones.

the tensile direction are submitted to local stretching whereas the lamellae parallel to the tensile direction are moved close due to the Poisson effect. Hence, the initial scattering ring turns into an oval-shaped one, indicating that the perpendicular long spacing L_p increases whereas parallel long spacing L_p decreases.

The evolution of the intensity scattered by the cavities is represented in Figure 1 by the arrows. From the initiation of the cavitation to a deformation ε of around 50%, the intensity scattered by the cavities is nonuniform: the spot is elongated in the horizontal direction of the pattern. This indicates that the cavities are not spherical but ellipsoidal and that they are oriented perpendicularly to the tensile direction.[19] Then, from 50%, the spot becomes more elongated in the vertical direction of the pattern, indicating that the cavities change their orientation and get longer along the tensile direction (see the schemes of the cavities in Figure 1). From 55% to 70%, the largest dimension of the elliptic cavities continues increasing.

In addition, a ring representing the crystallite diffusion can be observed. Close to the initiation of cavitation, a four-point pattern can be observed. This four-point diagram is generally characteristic of the first stage of plastic deformation.[20−22] Indeed, it indicates that the crystalline lamellae are sheared and tilted to a preferential orientation.

Quantification of the Shape and Orientation of the Cavities. To quantify this phenomenon of cavitation, the following analysis can be carried out. The scattered intensity can be written as follows:

$$I(q) \propto F^2(q)S(q) \tag{3}$$

with $F(q)$ the form factor and $S(q)$ the interference factor. If we consider that the cavities are distant from each other and randomly distributed, the interference function equals to 1 and the intensity $I(q)$ is directly proportional to the square of the form factor $F(q)$. The patterns observed during tensile tests indicate that the cavity shape is anisotropic. To describe easily the structure and to give an order of magnitude of the cavity dimensions, it can be chosen to assimilate the elliptic cavities to cylinders of revolution of diameter D and height L.

$F^2(q)$ of a cylinder of revolution of diameter D and height L is[19]

$$F^2(q,\gamma) = \left[\frac{\sin\left(\frac{1}{2}qL\cos\gamma\right)}{\frac{1}{2}qL\cos\gamma}\,2\frac{J_1\left(\frac{1}{2}qD\sin\gamma\right)}{\frac{1}{2}qD\sin\gamma}\right]^2 \tag{4}$$

It is convenient to factorize form factor in its perpendicular and parallel components by defining the wave vector components $q_\perp$ and $q_\parallel$, respectively, perpendicular and

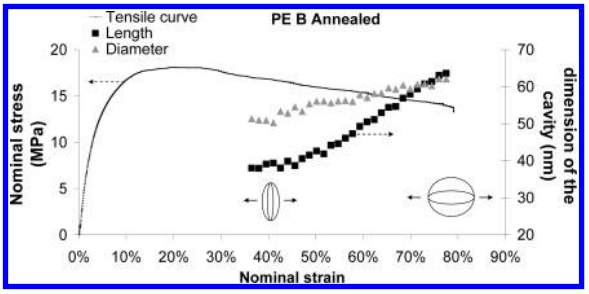

Figure 4. Tensile curve and evolution of the dimensions of the cavities of the PE B annealed.

parallel to the normal of the base of the cylinder:[23]

$$q_{\perp} = q \sin \gamma \tag{5}$$

$$q_{\parallel} = q \cos \gamma \tag{6}$$

with γ the angle between the normal of the base of the scattering cylinder and the wave vector q and J_1 the Bessel function of order 1.

In a perfectly oriented structure, we obtain

$$F^2(q_{\perp}, q_{\parallel}) = {F_{\parallel}}^2(q_{\parallel}){F_{\perp}}^2(q_{\perp}) = \left[\frac{\sin\left(\frac{1}{2}q_{\parallel}L\right)}{\frac{1}{2}q_{\parallel}L}\right]^2 \left[2\frac{J_1\left(\frac{1}{2}q_{\perp}D\right)}{\frac{1}{2}q_{\perp}D}\right]^2 \tag{7}$$

with ($q_{\perp} = q$ and $q_{\parallel} = 0$) when the scattering particle normal is perpendicular to the wave vector q and ($q_{\perp} = 0$ and $q_{\parallel} = q$) when the scattering particle normal is parallel to the wave vector q.

It can be noticed that usually this relation is approximated by Guinier's law.[19]

This relation emphasizes a possible anisotropy of the scattered intensity: first because L and D should be different, but also because of the two different functions (sin and J_1) for the two main directions. This calculation can be led since the intensity scattered by the cavities is strong enough and the cavities large enough to diffuse at small q values.

The intensity has been integrated over a quarter of $\pm 7.5°$ separately in the horizontal and vertical zones.

As an example, the diameter and the length of the cavities of the PE B annealed have been calculated and plotted against the nominal strain in Figure 4.

The anisotropy of the cavities is then quantified. Initially, the diameter is higher than the length, and thus the cavities are oriented perpendicularly to the tensile direction. The aspect ratio is here close to 1.25 at the beginning. Furthermore, it can be noticed that at the initiation of the cavitation the smallest dimension of the cavities is around 40 nm, which is higher than a long period (here 22 nm). It appears that the very first stages of nucleation can not be visible by SAXS as the phenomenon is nearly instantaneous: the cavity dimension evolves quickly from 0 to a critical value, around 40 nm. As the cavity dimensions are higher than the long period, it can be thought that when it nucleates, it causes at least a local fragmentation of the neighbored crystallites. The evolution of the cavity sizes observed in the X-rays observation window shows that the ellipsoids change their orientation: at the end of the neck, they are isotropic. We have observed that all the PE available in this study do all exhibit the same evolution of the shape and orientation of cavities, whatever their microstructure. There are however three exceptions: PE A annealed and quenched and PE B quenched. For these materials no cavitation has been observed along a tensile test.

For the PE that exhibits cavitation, the dimensions (L and D) are equal to 65 ± 5 nm for all the PE when the cavities recover an isotropic shape. Afterward, the cavities extend along the tensile direction. These results are in good agreement with several previous studies.[2,3]

Independently of these common features, several parameters seem to be strongly connected with the microstructural and molecular parameters: the initial size and aspect ratio of the cavities, the earliness of the apparition of the cavitation, the cavity volume and its evolution along tensile test, and finally whether a PE exhibits cavitation or not. In the following we will focus on the initiation of cavitation and cavity volume evolution.

Observation of Nucleation and Growth of the Cavities. To dissociate nucleation from growth, the evolution of the cavity volume can also be investigated and compared with the evolution of the dimensions of the cavities. In this case, the term of nucleation is used to describe the multiplication of the number of cavities.

In this aim, the intensity has been estimated using an azimutal integration angle ψ in the range $0 \le \psi \le 360°$. After the correction of the incident beam and the background, the intensity has been corrected by the sample thickness.

The PE D quenched has been chosen as a representative example to describe the evolution of the cavitation volume that has been found to be similar for all the polyethylenes which exhibit cavitation.

The intensity scattered by a given volume fraction of particles can be calculated with the following relation:[19]

$$2\pi^2 \Delta\rho^2 \phi(1-\phi) K_1 = \int_0^{\infty} I(q) q^2 \, dq \tag{8}$$

with $\Delta\rho$ the electronic density difference between the two different phases. Here, the density difference has been considered as it modifies only the value of the K_1 constant. ϕ is the volume fraction of one of the phase. For cavitation, this relation becomes

$$2\pi^2 {\rho_p}^2 V K_1 = \int_0^{\infty} I(q) q^2 \, dq \tag{9}$$

with ρ_p the density of the polyethylene and V the volume fraction of cavities (as the volume fraction is relatively small the above approximation can be done).

Here, to obtain the volume, the factor K_1 should be evaluated. The strategy employed consists in using the lamella scattering in the undeformed state so that no cavitation scatters the X-rays. For the lamella stacks, $\Delta\rho$ is the difference of density between crystal and amorphous phase $\Delta\rho = \rho_c - \rho_a$ ($\rho_c = 1.003$ and $\rho_a = 0.853$[8]). Moreover, the second term of relation 8 can be partitioned in three parts:

$$\int_0^{\infty} I(q) q^2 \, dq = \int_0^{q_1} I_{small}(q) q^2 \, dq + \int_{q_1}^{q_2} I(q) q^2 \, dq + \int_{q_2}^{\infty} I_{large}(q) q^2 \, dq \tag{10}$$

Assuming that

$$I_{small} = Aq + B \tag{11}$$

(the choice of this relation does not modify significantly the final results) and I_{large} following the law of Porod:

$$I_{large} = \frac{C}{q^4} \tag{12}$$

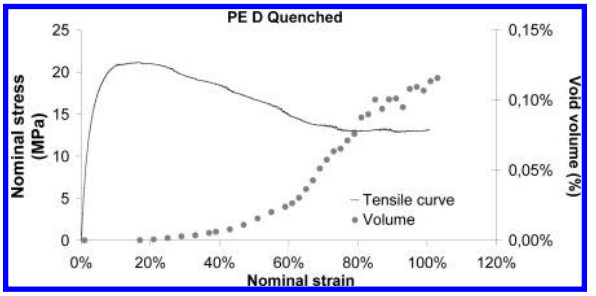

Figure 5. Tensile curve and evolution of the cavity volume against the nominal strain for the PE D quenched.

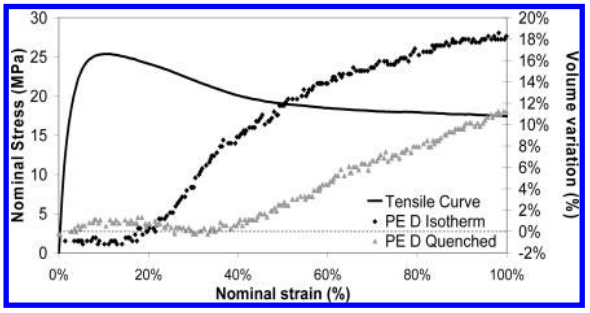

Figure 6. Volume variation of the PE D quenched and the PE D isotherm against the nominal strain obtained with a homemade dilatometer.

q_1 and q_2 are experimentally evaluated. They correspond to the q values at the beginning and at the end of the scattered peak. Then the integral between q_1 and q_2 can be calculated, and consequently the factor K_1 can be evaluated.

Therefore, the cavity volume fraction V can be calculated with the following relations:

$$V = \frac{1}{2\pi^2 \rho_p{}^2 K_1} \int_0^\infty I(q) q^2 \, dq \tag{13}$$

$$\int_0^\infty I(q) q^2 \, dq = \int_0^{q_{min}} I_{th}(q) q^2 \, dq + \int_{q_{min}}^{q_{max}} I_{exp}(q) q^2 \, dq + \int_{q_{max}}^\infty I_{th}(q) q^2 \, dq \tag{14}$$

with I_{exp} the experimental intensity, q_{min} the minimal measurable q ($q_{min} = 0.05$ nm^{-1}), and q_{max} chosen in order to have the lowest influence of the lamella stack scattering on the intensity ($q_{max} \sim 0.1$ nm^{-1}).

I_{th} is the theoretical intensity in a structure with randomly dispersed cavities. It has been calculated thanks to the cylinder model (eqs 7 and 3) by adjusting the parameters between q_{min} and q_{max}. It is worth noticing that an ellipsoid model would have here given the same results.

This analysis is based on an experimental measurement that can be performed in a limited window in the range of q_{min} and q_{max}. These values of q_{min} and q_{max} correspond to cavity dimensions approximately between 30 and 100 nm. Hence, we can only observe the cavities that pass through this window. As the cavities grow from their nucleation until they diffuse the visible light, they inevitably and temporally go through the observation window. At the initiation of the cavitation, the cavities exhibit a minimal size of 40 nm; thus, the observation window allows observing the exact state of the cavitation while all the cavities are not bigger than 100 nm. Then, after this initiation step, the observation window allows quantifying only the volume of the cavities which are included between 30 and 100 nm, at any moment of a tensile test. The cavity volume of the PE D quenched is plotted for each pattern along the tensile test against the nominal strain in Figure 5. In the undeformed state, a slight scattering is observed which could due to preexisting cavities or heterogeneities. Hence, all the values were translated in order to have a null value in the undeformed state.

It can be noticed that the values obtained by the SAXS calculation are very low. Usually, it is found that a HDPE could exhibit a volume strain up to 30%.[24] To check the order of magnitude, the volume variation of all the PE has been analyzed thanks to a homemade apparatus (cavitometer) design from the principle of the Farris dilatometer.[25] The volume variation of the PE D quenched and isotherm is plotted against the nominal strain up to the end of the neck in Figure 6.

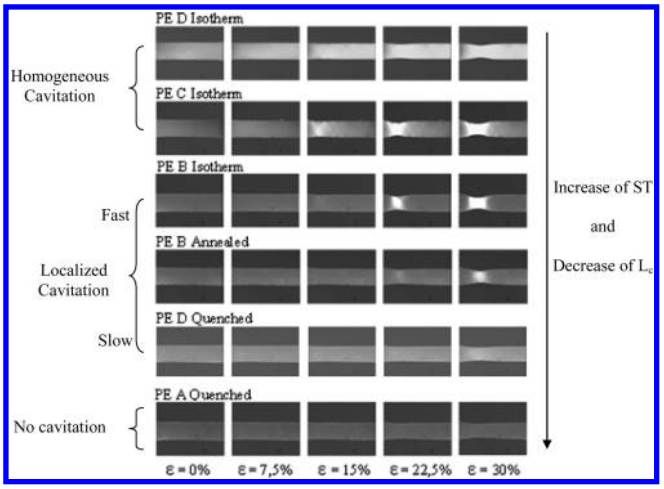

Figure 7. Observation of the sample macroscopic deformation and of the cavitation along a tensile test.

The classical order of magnitude is found. The difference of values obtained by SAXS and by dilatometer can be explained by the limitations of our SAXS devise presented before.

It is clear that the cavitometer is much more precise than the X-ray to quantify the cavity volume when the deformation is high. But it is impossible to determine precisely the initiation of cavitation as this apparatus gives the global volume change. The latter is very complex at the beginning of the deformation and is caused by cavitations, but also by the Poisson effect, reversible densification due to a strain-induced organization of the amorphous phase,[26] and even dilatation if the temperature is not kept perfectly constant.

On the contrary, the X-ray technique is very accurate and reliable to determine the cavity volume at the very beginning of cavitation. Afterward, the cavity volume calculated is the result of a competition between the new cavities that enter in the observation window and the older ones that exit it. Therefore, the SAXS results will be interpreted only in the initiation of cavitation when the large cavities do not exist yet.

Initiation of the Cavitation: Influence of the Microstructure. *Two Techniques To Observe the Cavity Formation.* Independently of the SAXS measurements, tensile tests have been performed. Pictures have been taken every 7.5% of deformation (see Figure 9). It allows following the macroscopic deformation and observing the presence of the cavitation.

A few hundred nanometer cavities are visible by whitening. In Figure 7, several mechanisms of initiation of cavitation are observed, depending on the considered PE.

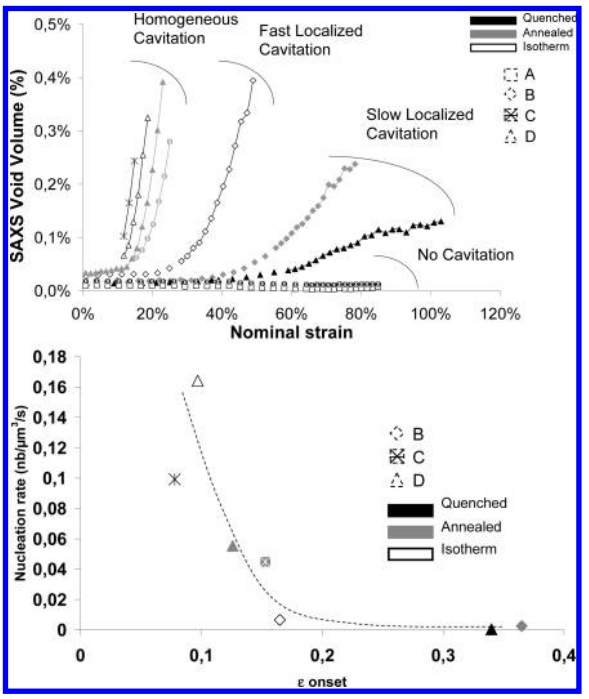

Figure 8. (a) Evolution of the cavity volume against the nominal strain of all the PE. (b) Determination of the nucleation rate for the materials for which it is possible.

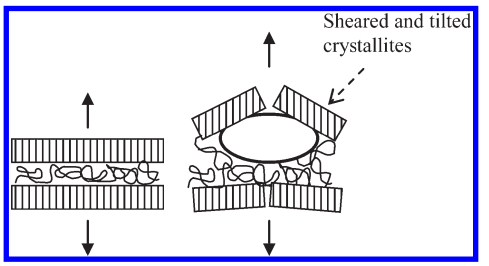

Figure 9. Scheme of the phenomenon of cavitation with its associated crystallite shearing.

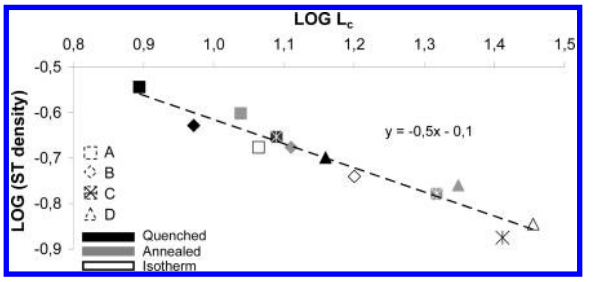

Figure 10. *ST* density ($1/\lambda_n$) against $\log(L_c)$.

- The PE D isotherm exhibits a homogeneous cavitation; that is to say, the cavities are formed all along the samples. The cavities are not localized and appear before the formation of the neck.
- The PE C isotherm exhibits a kind of homogeneous cavitation: the cavities appear along shear bands which are present in a large part of the sample. Then these shear bands become more intense at the place where the neck will be formed. Hence, the cavitation occurs before the initiation of the neck, as for the PE D isotherm.
- The PE B isotherm and annealed exhibit cavitation simultaneously with the formation of the neck, and the cavities are localized in the neck. Consequently, the cavitation can be qualified as localized. Furthermore, it can be noticed that cavitation and necking of the PE B annealed occur at higher nominal deformation than for the PE B isotherm and the PE D quenched. The PE D quenched does whitening, but at higher deformation than 30% (35%).
- The PE A quenched does not exhibit any visible cavitation, even during the formation of the neck which is much more diffuse.

Besides, the evolution of the cavity volume measured by SAXS along the tensile test for each PE is plotted against the nominal strain in Figure 8a. The different cavitation behaviors observed in Figure 7 are confirmed by SAXS measurements in Figure 10. Furthermore, it appears that the sooner the cavitation is initiated, the faster the nucleation of the cavities is (the higher the slope of the curves is), and so the more significant the increase in volume is.

It can be noticed that it has been checked that the incident beam was irradiating the place where the neck was initiated. Indeed, the gauge length of the sample was very small, and the neck was always initiated in the center of the sample.

These measurements allow evaluating the onset of cavitation (ε_{onset}). A tangent method has been used: the slope at the very beginning of the curve and the slope just after the loss of linearity have been considered. The intersection gives the ε_{onset}. For example, the ε_{onset} of the PE D isotherm is close to 10%. To determine the onset of cavitation, we use the nominal deformation $\varepsilon = \Delta L/L_0$. Indeed, the in-situ tensile device for X-ray is very small and does not allow a local measurement of the true deformation. Locating a physical phenomenon with this indicator does not give absolute information as it is dependent on the shape of the sample, the strain rate, and the temperature. However, it allows comparing our materials.

Figure 8b is deduced from Figure 8a and the ε_{onset}. The nucleation rate is determined by measuring the slope at the very beginning of the cavity volume increase. Indeed, it is assumed that this increase is representative only of cavity nucleation as no cavity should have exit the SAXS window yet. Second, this volume is divided by the volume of a single cavity determined with the characteristic dimensions obtained before. It is supposed here that the distribution of size is relatively small at the beginning. The nucleation rate is thus a number of cavities per μm^3 and per second. This nucleation rate is of course dependent on the strain rate. It can be underlined that the nucleation rate range is rather important as it is multiplied by a factor 100 comparing PE D isotherm and PE B annealed. Moreover, for the others materials (PE A, for example), the nucleation rate cannot be measured as they do not cavitate. However, for few materials it is possible to determine approximately the onset due to a very little slope variable in the cavity volume measured even if the slope cannot be measured accurately.

Discussion: Homogeneous versus Localized Cavitation. The initiation of the cavitation has been studied by Pawlak and Galeski.[3] They suggest that it exists a competition between two processes: the cavitation in the amorphous phase and the plastic deformation in the crystal. In this work, it is supposed that, at a fixed stress, close to the macroscopic yield stress, if the local stress σ_{cav} is lower than the local stress σ_{sh} necessary to shear a crystallite, then the initiation of cavitation should occur first and thus should be the origin of the macroscopic yield. Furthermore, it is supposed that, if the cavitation is not initiated before the crystallite shearing, then it will not occur after.

These assumptions are consistent with the SAXS pattern of the PE B annealed. Indeed, in Figure 1, at $\varepsilon = 30\%$, it appears that beside the presence of cavitation, a four-point

pattern can also be observed. This four-point pattern indicates that the crystalline lamellae are sheared and tilted to a preferential orientation. It can be concluded that the plastic deformation of the crystallites and the cavitation are linked (see Figure 9). The fact that the yield stress is higher in compression than in tension also demonstrates the influence of the cavitation on the macroscopic yield.[3] However, it can only be concluded that the cavitation accelerates the crystallite shearing, which decreases the yield stress value. But it can not be concluded if the cavitation occurs before or after the shearing of several crystallites.

To be able to explain all the cavitation scenarios observed on the different PE, a hypothesis have to be done on the cavitation stress σ_{cav}. The classical theory of nucleation process which implies the contribution of a surface and volume energy can be used.[27−29] The latter has been adapted by Mourglia[30,31] to model cavitation in polyamide. This is a physical-based approach that helps to describe simply the initiation of cavitation in order to obtain a realistic hypothesis for the cavitation stress.

The energy of the material and the cavities is supposed to be given by

$$\psi = -\alpha B\varepsilon_v{}^2 r^3 + \beta\gamma r^2 \tag{15}$$

where B is the compressibility modulus, ε_v is the volume deformation, γ is the surface tension, r is the radius of a spherical cavity, and α, β are proportionality coefficients.

The first term represents the elastic volume energy relaxed by the formation of cavities and the second (unfavorable to cavitation) the surface energy.

As the cavitation is assumed to occur in the amorphous phase, the local volume deformation can be related to the local stress σ and amorphous modulus E_a by

$$\varepsilon_v \propto \varepsilon = \frac{\sigma}{E_a} \tag{16}$$

Therefore, the energy of the system becomes

$$\psi = -\alpha B \frac{\sigma^2}{E_a{}^2} r^3 + \beta\gamma r^2 \tag{17}$$

A high modulus of the amorphous phase is unfavorable to the formation of a cavity. The amorphous modulus is not well-known; however, according to Boyd,[32] crystallization conditions should strongly affect the amorphous modulus value. The latter would depend on tie molecules, entanglements, interphase, and of course temperature. For us, all these parameters can be gathered in the ST parameter so that we suppose here that

$$E_a = E_1 + \alpha_2 ST \tag{18}$$

where E_1 and α_2 are constant. In addition, a large range of value has been found in the literature.[8,32] When considering the ST influence and the value of the amorphous modulus, it can even reach 300 MPa, which is strongly higher than the modulus of a bulk rubber. Consequently, E_1 should be significantly lower than $\alpha_2 ST$.

Even if it can be supposed that cavity nucleation is easier at the interface between crystal and amorphous phase, elements as tie molecules reinforce strongly this interface and then prevent the formation of cavities. Therefore, this approach remains qualitatively true.

The definition of such a potential allows determining a critical radius; then a potential barrier which corresponds to the energetic gap when the radius evolves from 0 to the critical radius. The potential barrier is given here by

$$\Delta\Psi = \frac{4\gamma^3\beta^3(E_1 + \alpha_2 ST)^4}{27\alpha^2 B^2\sigma^4} \tag{19}$$

A characteristic time of nucleation can be obtained using a thermically activated law:

$$\tau = \tau_0 \exp\left(\frac{\Delta\Psi}{kT}\right) \tag{20}$$

where k is the Boltzmann constant and τ_0 is a reference time.

For a given nucleation time, the stress can be expressed in relation with the others parameters of the problem by using eqs 19 and 20:

$$\sigma_{cav} = C(E_1 + \alpha_2 ST) \tag{21}$$

with $C = f(k, T, \tau, \tau_0, B, \alpha, \beta, \gamma)$.

When setting the temperature and the modulus, C is a new constant including in particular the given nucleation time. The stress σ_{cav} is then required to obtain a cavitation in the given nucleation time. Therefore, it can be associated with the cavitation stress (labeled σ_{cav}). Even if the correlation found between σ_{cav} and ST was quite intuitive, it is interesting to notice that it is compatible with the nucleation theory.

Besides, as proposed in a previous work,[6] the initiation of the crystallite shearing should be described by a function of the critical macroscopic tensile stress σ_c and the density of stress transmitters ST. The macroscopic threshold stress σ_{th}, necessary to initiate the crystallite shearing and thus the plastic deformation, is defined as

$$\sigma_{th} = k'\left(\frac{\sigma_c}{\sigma_{c_0}}\right)\left(\frac{ST}{ST_0}\right)^{\beta} \tag{22}$$

with

$$\sigma_c = f(T)\exp -\left[\frac{2\pi\Delta G_c}{Klb^2} + 1\right] \tag{23}$$

with b the magnitude of the Burgers vector, l the stem length, r_0 the core radius of dislocation, E_0 the core energy, ΔG_c the critical value of the Gibbs free energy, K the crystalline shear modulus, and $f(T)$ a function of the temperature. β was found to be equal to 0.6.

Over a range of L_c within 10−30 nm a good approximation of this relation leads to a proportional relation between σ_c and L_c (or the stem length l). The local stress σ_{sh} applied on the crystallite should follow the same evolution than the macroscopic threshold stress $\sigma_{th.}$

Then the two following simplifications can be used:

$$\sigma_c \propto L_c \tag{24}$$

and

$$\sigma_{sh} \propto \sigma_{th} \tag{25}$$

If $\sigma_{sh} < \sigma_{cav}$, the crystallite shearing should occur first, before the cavitation. Consequently, it seems judicious to compare σ_{sh} and σ_{cav} in relation with the microstructure of the materials in order to conclude on the preferential activated mode.

To compare σ_{sh} and σ_{cav}, it is convenient to limit the description of the microstructure to a unique parameter. The most adequate seems to be the crystallite thickness L_c. As σ_{cav} and σ_{sh} are defined in relation with ST and L_c, the correlation between ST and L_c is required.

In Figure 10, a very good correlation can be observed between the ST density and L_c. ST can be then described by

$$ST \propto \left(\frac{1}{L_c}\right)^{0.5} \tag{26}$$

Therefore, it leads that

$$\sigma_{cav} \propto E_1 + \alpha_2 ST \propto E_1 + \alpha_2 \left(\frac{1}{L_c^{0.5}}\right) \tag{27}$$

And when combining the relations 22, 24, 25, and 26, it leads to express σ_{sh} as follows:

$$\sigma_{sh} \propto L_c \left(\frac{1}{L_c^{0.5}}\right)^{0.6} \propto L_c^{0.7} \tag{28}$$

Despite of all the approximations, the important point is that σ_{cav} increases with L_c whereas σ_{sh} decreases. In this condition the following analysis remains valid. The schematic evolution of σ_{sh} and σ_{cav} is plotted against L_c in Figure 11.

When σ_{sh} is inferior to σ_{cav} ($0 < L_c < L_{cc}$), the crystallite shearing is the first phenomenon that occurs, whereas above L_{cc}, σ_{cav} is inferior to σ_{sh} and thus the cavitation occurs first. The intersection of the two curves (L_{cc}) represents a critical value of L_c. The value of L_{cc} depends on the experimental temperature and strain rate as at least σ_{sh} depends strongly on these both experimental parameters.

Experimentally, it is found, at ambient temperature and at a strain rate of 5×10^{-3} s^{-1}, that L_{cc} is around 19 nm: for the PE B isotherm ($L_c = 16$ nm) the crystallite shearing occurs first, whereas for the PE C annealed ($L_c = 21$ nm) the cavitation occurs first.

Scenario of Homogeneous Cavitation. Let us consider a sample with a crystallite thickness L_c such as $L_c \gg L_{cc}$ (Figure 12A).

Along the tensile test the local stress σ_{local} increases. It is assumed that $\sigma_{cav} < \sigma_{sh}$. Under σ_{cav}, the behavior of the material is viscoelastic: neither the crystallite shearing nor the cavitation occurs. When σ_{local} exceeds σ_{cav}, the cavitation can be initiated. This particular case is observed for the PE D isotherm and the PE C isotherm that exhibit homogeneous cavitations. Furthermore, it can be supposed that the cavitation increases the stress concentration in the neighborhood of the crystalline lamellae.[2] It would imply a local stress jump upper to σ_{sh}. This mechanism explains that the samples that exhibit a homogeneous cavitation are then quickly submitted to necking. Furthermore, we have seen that the dimensions of the cavity become quickly superior to the long period. Thus, it can explain that when a cavity is nucleated, it favors the development of plasticity. In this scenario, cavitation is a part of the cause of the initiation of plasticity.

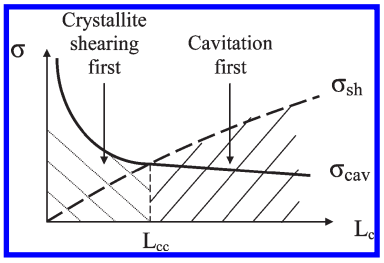

Figure 11. Schematic evolution of σ_{sh} and σ_{cav}.

Scenario of Localized Cavitation. Let us suppose now a sample with a crystallite thickness $L_c < L_{cc}$ (see Figure 12B). In this case, $\sigma_{sh} < \sigma_{cav}$. Under σ_{sh}, the behavior of the materials is viscoelastic: neither the crystallite shearing nor the cavitation occurs. When exceeding σ_{sh}, the crystallite shearing can be initiated and so is the macroscopic neck formation. This particular case is observed for the PE B annealed and isotherm for example. Furthermore, it can be supposed that the crystallite shearing increases the stress concentration in the neighborhood of the crystalline lamellae. It implies a local stress jump increasing σ_{local} upper to σ_{cav}. This mechanism explains that the samples that exhibit first necking then they quickly void. In this scenario, crystallite shearing is a part of the cause of the initiation of cavity formation.

Absence of Cavitation. The case of a sample with a crystallite thickness L_c such as $L_c \ll L_{cc}$ is represented in Figure 12C. When exceeding σ_{sh}, the crystallite shearing is initiated. Quickly, the macroscopic neck formation follows. However, as the gap between σ_{sh} and σ_{cav} is significant, the stress concentration involved by the crystallite shearing is not sufficient to increase σ_{local} in such way to reach σ_{cav}. In this case, cavitation cannot occur.

This particular case is observed for the PE A quenched for example.

Prediction of the Initiation of Cavitation. The above analysis is only based on the stresses that induce cavitation. To compare it to the measured ε_{onset}, we propose a simple approach. First, in the elastic domain, when dividing by the modulus of the material E, ε_{onset} should be obtained.

$$\frac{\sigma_{cav}}{E} = \varepsilon_{onset} \propto \frac{E_1 + \alpha_2 ST}{E} \tag{29}$$

Over a range of L_c within 10−30 nm, E is assumed to be linear with L_c

$$\varepsilon_{onset} \propto \frac{E_1 + \alpha_2 ST}{\beta_1 + \beta_2 L_c} \tag{30}$$

where β_1 and β_2 are constant.

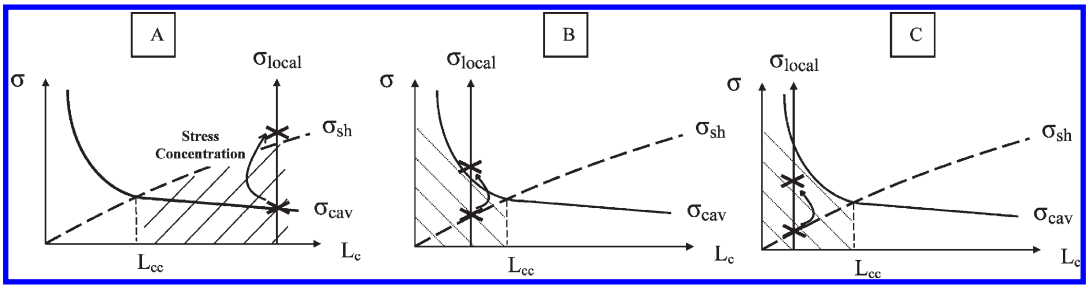

Figure 12. Schemes of the three different processes of cavitation: homogeneous (A) and heterogeneous cavitation (B) and absence of cavitation (C).

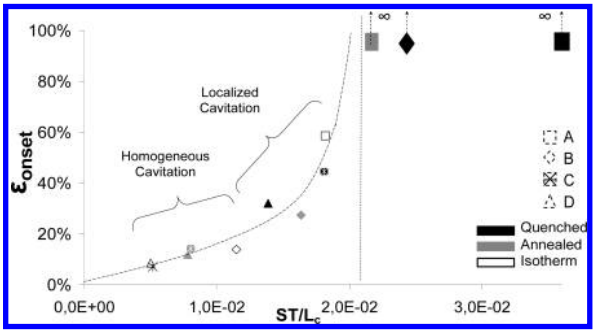

Figure 13. ε_{onset} against the ratio ST/L_c.

This expression could be also expressed only in relation with L_c, but here it seems more meaningful to keep the contribution of ST and L_c since σ_{cav} increases with ST and E with L_c. When simplifying eq 30 by eq 31

$$\varepsilon_{onset} \propto ST/L_c \tag{31}$$

The monotony of ε_{onset} is not affected, and therefore ST/L_c can be taken as a good indicator of initiation of cavitation.

In Figure 13, ε_{onset} is then plotted against ST/L_c. A good correlation is highlighted. Furthermore, a limit of cavitation is also highlighted: $ST/L_c \approx 0.02$, which corresponds to crystallite thickness of about 11−12 nm. Over this value, no cavitation can occur ($\varepsilon_{onset} \rightarrow \infty$) as σ_{cav} has never been reached. Heterogeneous and homogeneous cavitation appears in separate zones. Indeed, eq 31 is a good approximation in the elastic domain (for homogeneous cavitation). On the contrary, it becomes incorrect for heterogeneous cavitation which is consistent with the divergence of the curve just before the limit of cavitation. However, the hierarchy is respected because the yield stress generally grows with crystallinity.

Conclusion

The phenomenon of cavitation has been widely studied as it can affect the yield stress and the properties for large strains. In this work, the direct influence of the microstructural and molecular parameters on cavity formation has been accurately investigated with a special attention on the initiation of cavitation and the nucleation rate.

A wide range of microstructural parameters and stress transmitters density has been obtained from various polyethylenes. Thanks to SAXS in-situ tensile tests, the nucleation rate has been followed up. We have shown that this rate can evolve over several orders of magnitude and even until insignificant value for high ST density PE (for example, branched and quenched PE).

It is found that the phenomenon of cavitation can appear with three different scenarios: some PE exhibit homogeneous cavitation that consists in the formation of cavities all along the sample; others exhibit heterogeneous cavitation localized in the neck, and others do not exhibit cavitation.

The preferential activated mode depends on the respective values of σ_{cav} and σ_{sh}. Two models have made possible the understanding of their evolution in relation with microstructural parameters. They are based on nucleation theory, thermal activation, and, on the other hand, crystallite shearing. They allow relying σ_{cav} and σ_{sh} to the stress transmitter density and then to crystallite thickness. A critical value of crystallite thickness (L_{cc} = 19 nm in the specified conditions) has been found.

Above L_{cc}, σ_{cav} is lower than σ_{sh}; therefore, the cavitation is initiated before the crystallite shearing. This is the case for the homogeneous cavitation. The cavitation increases the local stress, favoring the plasticity and thus the yield stress appears earlier.

Below L_{cc}, σ_{sh} is lower than σ_{cav}, and the cavitation is heterogeneous; therefore, the crystallite shearing is initiated before the cavitation. Afterward, the plasticity increases the stress concentration which favors the nucleation of cavities. If this increase is not high enough, the cavitation cannot be initiated. This is the case for the PE exhibiting a crystallite thickness lower than 12 nm (at ambient temperature and strain rate used here).

Finally, the evolution of initiation of cavitation (ε_{onset}) has been qualitatively explained by the crystallite thickness and the ST density.

Surprisingly, our results have shown that all the scenarios of plasticity and cavitation are possible. One is the cause or the consequence of the other in accordance with the molecular topology and the thermal treatments. All theses scenarios have been explained by a simple model based on very few microstructural parameters.

Acknowledgment. Jenny Faucheu and Emilie Planes are thanked for their help in the experiments at the ESRF.

References and Notes

(1) Butler, M. F.; Donald, A. M.; Ryan, A. J. *Polymer* **1998**, *39* (1), 39–52.
(2) Pawlak, A. *Polymer* **2007**, *48* (5), 1397–1409.
(3) Pawlak, A.; Galeski, A. *Macromolecules* **2005**, *38* (23), 9688–9697.
(4) Schneider, K.; Trabelsi, S.; Zafeiropoulos, N.; Davies, R.; Riekel, C.; Stamm, M. *Macromol. Symp.* **2006**, *236* (1), 241–248.
(5) Kazmierczak, T.; Galeski, A.; Argon, A. S. *Polymer* **2005**, *46*, 8926−8936.
(6) Humbert, S.; Lame, O.; Vigier, G. *Polymer* **2009**, *50* (15), 3755–3761.
(7) Young, R. J. *Philos. Mag.* **1974**, *30*, 85–94.
(8) Crist, B.; Fisher, C. J.; Howard, P. R. *Macromolecules* **1989**, *22* (4), 1709–1718.
(9) Brooks, N. W.; Ghazali, M.; Duckett, R. A.; Unwin, A. P.; Ward, I. M. *Polymer* **1999**, *40* (4), 821–825.
(10) Séguéla, R. *J. Polym. Sci., Part B: Polym. Phys.* **2002**, *40* (6), 593–601.
(11) Nikolov, S.; Raabe, D. *Polymer* **2006**, *47*, 1643–1703.
(12) Butler, M. F.; Donald, A. M.; Ryan, A. J. *Polymer* **1997**, *38* (22), 5521–5538.
(13) Castagnet, S.; Deburck, Y. *Mater. Sci. Eng., A* **2007**, *448* (1−2), 56–66.
(14) Huang, Y. L.; Brown, N. *J. Polym. Sci., Part B: Polym. Phys.* **1991**, *29* (1), 129–137.
(15) Huang, Y. L.; Brown, N. *J. Mater. Sci.* **1988**, *23*, 3648–3655.
(16) Séguéla, R. *Macromol. Mater. Eng.* **2007**, *292* (3), 235–244.
(17) Seguela, R. *J. Polym. Sci., Part B: Polym. Phys.* **2005**, *43* (14), 1729–1748.
(18) Hubert, L.; David, L.; Séguéla, R.; Vigier, G. *Polym. Int.* **2004**, *53* (5), 582–585.
(19) Guinier, A.; Fournet, G. *Small-Angle Scattering of X-Rays*; Wiley: New York, 1955.
(20) Peterlin, A.; Balta-Calleja, F. J. *J. Appl. Phys.* **1969**, *40* (11), 4238–4242.
(21) Wang, W.; Murthy, N. S.; Grubb, D. T. *Polymer* **2007**, *48* (12), 3393–3399.
(22) Gerasimov, V. I.; Genin, Y. V.; Tsvankin, D. Y. *J. Polym. Sci., Polym. Phys. Ed.* **1974**, *12* (10), 2035–2046.
(23) Van Der Beek, D.; Petukhov, A. V.; Davidson, P.; Ferre, J.; Jamet, J. P.; Wensink, H. H.; Vroege, G. J.; Bras, W.; Lekkerkerker, H. N. W. *Phys. Rev. E* **2006**, *73* (4), 041402.
(24) Addiego, F.; Dahoun, A.; G'Sell, C.; Hiver, J.-M. *Polymer* **2006**, *47* (12), 4387–4399.
(25) Ramier, J.; Chazeau, L.; Gauthier, C.; Stelandre, L.; Guy, L.; Peuvrel-Disdier, E. *J. Mater. Sci.* **2007**, *42*, 8130–8138.
(26) Gaucher-Miri, V.; Depecker, C.; Séguéla, R. *J. Polym. Sci., Part B: Polym. Phys.* **1997**, *35* (13), 2151–2159.

(27) Christian, J. W. *The Theory of Transformation in Metals and Alloys: An Advanced Textbook in Physical Metallurgy*, 2nd ed.; Pergamon: Oxford, 1975.
(28) Kelton, K. F. In *Solid State Physics*; Ehrenreich, D. T., Ed.; Academic Press: New York, 1991; Vol. *45*, pp 75−177.
(29) Kashchiev, D. *Nucleation: Basic Theory with Applications*; Butterworth Heinemann: Oxford, 2000.
(30) Mourglia-Seignobos, E.; Long, D.; Odoni, L.; Sotta, P.; Vanel, L.; Rochas, C.; Narayanan, T., submitted to *Macromolecules* **2010**.
(31) Mourglia, E. *Compréhension des mécanismes physiques de fracture dans le Polyamide vierge et renforcé fibres de verre*; INSA: Lyon, 2009.
(32) Boyd, R. H. *Polym. Eng. Sci.* **1979**, *19* (14), 1010–1016.